

Fast voltage boosters to improve transient stability of power systems with 100% of grid-forming VSC-based generation

Régulo E. Ávila-Martínez¹, Javier Renedo¹, Luis Rouco¹, Aurelio García-Cerrada¹, Lukas Sigríst¹, Taoufik Qoria², and Xavier Guillaud²

¹Instituto de Investigación Tecnológica (IIT), ETSI ICAI, Universidad Pontificia Comillas, Madrid, Spain

²Laboratoire d'Electrotechnique de Puissance (L2EP), Centrale Lille, Arts et Métiers Paris Tech, University of Lille, Lille, France

Abstract

Grid-forming voltage source converter (GF-VSC) has been identified as the key technology for the operation of future converter-dominated power systems. Among many other issues, transient stability of this type of power systems remains an open topic of research because it is still a key limiting factor for stressed power systems. Previous studies have proposed control strategies for GF-VSC to improve transient stability of this type of systems by suitable current-limitation algorithms and/or control of active-power injections. As an alternative, this paper proposes two fast voltage boosters to improve transient stability of power systems with 100 % of GF-VSC-based generation with virtual synchronous machine (VSM). One control strategy uses local measurements, whereas the other one uses global measurements of the frequency of the centre of inertia (COI). Both strategies improve transient stability of this type of systems significantly. The advantage of using fast voltage boosters for this purpose is that the set points linked to frequency/active-power injection (i.e set points linked to the primary energy source of the VSCs) will not be modified. Furthermore, strategies such as current-limitation, active-power control and fast voltage controllers for transient stability improvement are compatible and complementary.

Index terms: Voltage source converter, VSC, grid forming, transient stability

This is an unabridged draft of the following paper (submitted to IEEE Transactions on Smart Grid on 4-6-2021):

- R. E. Ávila-Martínez, J. Renedo, L. Rouco, A. García-Cerrada, L. Sigríst, T. Qoria, X. Guillaud, "*Fast voltage boosters to improve transient stability of power systems with 100% of grid-forming VSC-based generation*", Manuscript ID: TSG-00871-2021, pp. 1-8, 2021.
- Internal reference of this paper: IIT-21-078WP.

1 Introduction

Future power systems are planned for massive integration of renewable energy sources. Non-conventional renewable generators, such as wind turbines and solar photovoltaic (PV) generators are interfaced through voltage source converters (VSC). Grid-forming VSC (GF-VSC) has been identified as the key technology for the operation of future converter-dominated power systems, from small microgrids [1–3] to large transmission systems [4, 5]. The main characteristic of a GF-VSC (also known as voltage-controlled VSC) is that it controls its output voltage magnitude and frequency and therefore, it is capable of creating a grid. This is not possible with most extended grid-following VSCs (also known as current-controlled VSCs or grid-feeding VSCs). When operating a power system with several GF-VSCs, they need a self-synchronisation mechanism, in order to ensure that all of them reach the same frequency. Fortunately, unlike in grid-following VSCs, synchronisation can be achieved without using a phase-locked loop (PLL) by means of supplementary control strategies. Although there are variants of these supplementary control strategies, the philosophy behind most of them is that they control GF-VSCs in order to mimic the behaviour of conventional synchronous generators. The most common option in alternating-current (AC) microgrids is the so-called power-frequency (P-f) droop [1–3], while the most common option in large power systems is the emulation of synchronous machines, in the so-called synchroconverters [6] or virtual synchronous machines (VSM) [7, 8]. Furthermore, the work in [9] proved that P-f droop supplementary controllers and VSM supplementary controllers are equivalent. A different approach for self-synchronisation of GF-VSCs is the concept of reactive-power synchronisation, proposed recently in [10].

Transient stability (or angle stability with large disturbances) is defined as the ability of the generators of the system to remain in synchronism when large disturbances occur [11]. Initially, this definition assumed that the system contains synchronous generators, since the phenomenon is related to the rotor angle of synchronous machines. However, recent publications have shown that transient stability is also a concern in power systems with 100% of GF-VSC-based generation. In other words, if GF-VSCs emulate synchronous machines, they can also lose synchronism in case of severe-enough faults.

The work in [12,13] observed that the loss-of-synchronism phenomenon can occur in AC microgrids with GF-VSC generators equipped with P-f droop control; transient stability was assessed by means of Lyapunov’s theory. Further studies are presented in [14,15], where the impact of current saturation [14] and fault-ride-through (FRT) capability [15] of GF-VSCs on transient stability is analysed. References [16,17] analysed transient stability in power systems with GF-VSC controlled as VSMs. The study in [17] included experimental results. A similar approach is followed in [18], where a thorough analysis of transient stability of GF-VSCs is provided, and it also includes experimental results. The work in [19] analyses the impact of current-limiting strategies on transient stability of a GF-VSC connected to an infinite grid. The study analyses two current-limiting strategies: the conventional current limiter for the current modulus in vector control and virtual-impedance-based current limiter. Eventually, the work proposes an hybrid current limiter which is a combination of both, improving the performance of the current limitation process as well as transient stability. The work in [20] goes a step further and analyses transient stability of a GF-VSC connected to an infinite grid, using virtual-impedance current limiters of the GF-VSC. The work proposes an adaptative droop in the GF-VSC by changing the proportional gain of the P-f droop controller during the fault. Results show that the strategy increases the critical clearing time (CCT) of a fault, significantly. The work in [21] proposed an adaptive emulated inertia in the GF-VSC in order to improve transient stability. The three studies [19–21] include experimental results. Reference [22] analysed the case of a GF-VSC (with VSM) and a grid-following VSC connected to an infinite grid. The study proposed a control strategy for the grid-following VSC for transient stability disabling the PLL of the grid-following VSC during the fault and using, instead, remote measurements to obtain the virtual rotor angle of the GF-VSC and use it for vector control of the grid-following VSC. The work in [23] analysed transient stability of a power system with 100% of GF-VSC-based generators working like VSMs. The work proposed an active-power (P) control strategy based on a PI controller using, as input signal, the frequency deviation with respect to the frequency of the centre of inertia (COI), in order to improve transient stability and producing promising results. The work in [24] proposes a supplementary P-control strategy proportional to the frequency deviation with respect to the nominal frequency (using local measurements) to improve transient stability of a GF-VSC connected to an infinite grid. The study provides guidelines for the design of the proposed controller and it includes experimental results.

The research studies described above have shown that transient stability in power systems with GF-VSCs can be improved (a) by implementing suitable current limiters [19, 20] or (b) by implementing suitable active-power-

related control strategies [19–21,23]. However, the use of control strategies based on reactive-power (Q) injections or voltage control to improve transient stability in power systems with 100 % of GF-VSC-based generation has not been investigated in previous work. Furthermore, the use of reactive-power/voltage control strategies to improve transient stability have been successfully applied in traditional synchronous generators (i.e. excitation boosters) [25–30], in shunt FACTS devices [31] and in high voltage direct current systems based on voltage source converters (VSC-HVDC) [32,33]. The good results obtained there, has motivated this research.

An important advantage of controlling voltage at the output of the filter of the GF-VSC is that the converter will change its reactive-power injection, while the set points linked to frequency/active-power injection will not be modified. In other words, this type of controllers do not involve changing the set point of the primary energy source of the GF-VSC. Along this line, this work proposes two control strategies based on fast voltage boosters to improve transient stability in power systems with 100% of GF-VSC-based generation. One control strategy uses local measurements, whereas the other one uses global measurements of the frequency of the COI. Both strategies improve transient stability of this type of systems significantly.

Specifically, the contributions of this work are as follows:

- Proposal of two fast voltage boosters to improve transient stability of power systems with 100% of GF-VSC-based generation, one based on local measurements and the other one based on global measurements.
- Significant improvements on the critical clearing times of different faults, thanks to the two control strategies.
- Analysis of the impact of communication latency on the performance of the proposed global control strategy. Results show that the proposed control strategy is robust for realistic communication latency.
- Discussion about the use of local and global measurements in this type of controllers.

2 Grid-forming VSCs

2.1 Modelling and control

This section describes the model of a GF-VSC, following the guidelines of [5,21,34–36]. Fig. 1 shows the equivalent model of a GF-VSC- i . The converter is represented as a voltage source ($\bar{e}_{m,i}$) and it is connected to the rest of the system through an LC filter, consisting of a phase reactor ($\bar{z}_{f,i} = r_{f,i} + j\omega_i L_{f,i}$) and a capacitor ($\bar{z}_{c,i} = -j/(\omega_i C_{f,i})$), and a transformer ($\bar{z}_{c,i} = r_{c,i} + j\omega_i L_{c,i}$).

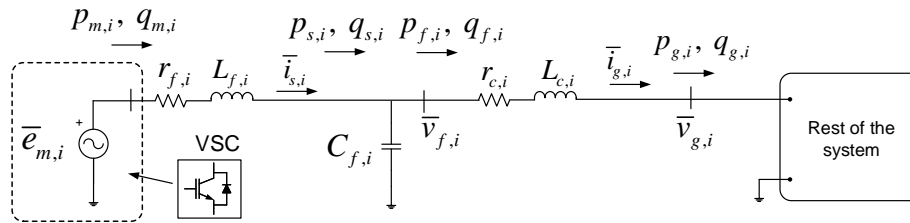


Figure 1: Model of a grid-forming VSC.

The GF-VSC- i will control:

- The magnitude of the voltage at bus f : $v_{f,i}$.
- The frequency at bus f : $\omega_{f,i}$. This means that the VSC controls the angle of the voltage at bus f : $\delta_{f,i}$.

Fig. 2 shows the general control structure of a GF-VSC- i based on vector control [21,35]. It consists of: (a) a voltage controller, (b) a virtual transient resistance, (c) a current controller, (d) voltage modulation and (e) a grid-forming mechanism for self-synchronisation (e.g. VSM or any other variant). The details of the control system can be found in [5,21,34–36]. Hence, only a summary is provided here.

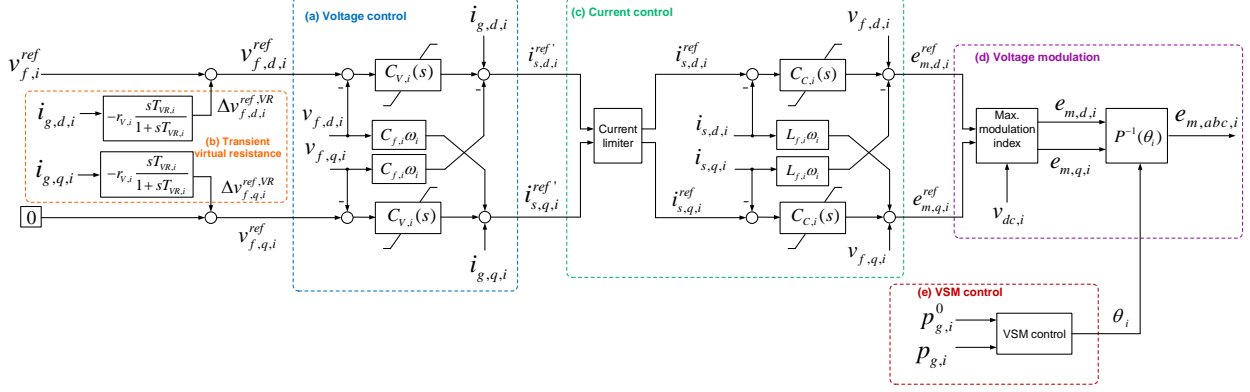


Figure 2: General scheme of the control system of a grid-forming VSC.

First of all, the VSC imposes an angle δ_i (rad) for the mobile $d-q$ reference frame which rotates at a speed ω_i (pu), as illustrated in Fig. 3. The angle δ_i is referred to an arbitrary mobile $R-I$ reference frame rotating at the synchronous frequency. The position of the d axis with respect to a static reference frame (angular speed equal zero), θ_i , is the one used in Park's Transform to refer variables to the $d-q$ reference frame. The way in which this angle is obtained from the self-synchronisation method (VSM control in Fig. 2) will be described in Section 2.2.

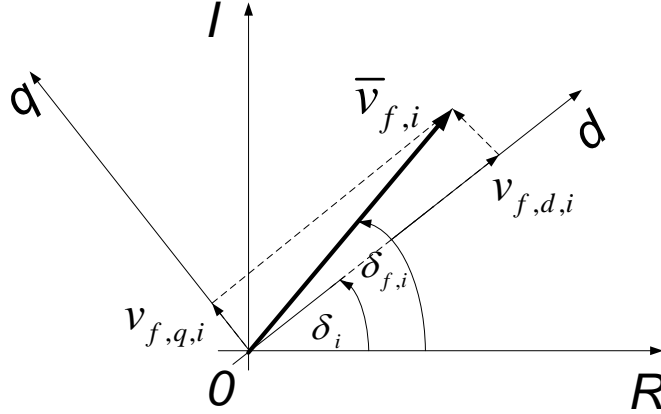


Figure 3: Grid-forming VSC: $d-q$ axes.

The voltage control loop (Fig. 2) controls $v_{f,d,i}$ and $v_{f,q,i}$ with proportional-integral controllers (PI) where set-point values are given by:

$$\begin{aligned} v_{f,d,i}^{ref} &= v_{f,i}^{ref} + \Delta v_{f,d,i}^{ref,VR} \\ v_{f,q,i}^{ref} &= 0 + \Delta v_{f,q,i}^{ref,VR} \end{aligned} \quad (1)$$

where $v_{f,i}^{ref}$ is the set point of the magnitude of the voltage and $v_{f,q,i}^{ref}$ is controlled to zero. $\Delta v_{f,d,i}^{ref,VR}$ and $\Delta v_{f,q,i}^{ref,VR}$ represent the transient virtual resistance: they only have impact during transients and are used for damping [35]. Eventually, the voltage controller aligns the voltage $\bar{v}_{f,i}$ with the $d-q$ axes of the VSC (see Fig. 3).

The outputs of the voltage controller are the set points of $d-q$ current components of the current controllers, which have a current limiter and PI controllers. The current limiter is implemented with the conventional current saturation algorithm used in vector control [19] (i.e. the modulus of the current vector is limited). The outputs of

the current controllers are the modulated voltages $e_{m,d,i}$ and $e_{m,q,i}$, related to the DC voltage as:

$$\bar{e}_{m,i} = \bar{m}_i v_{dc,i}, \quad \text{with } e_{m,i} \leq m_i^{max} v_{dc,i} \text{ (pu)}. \quad (2)$$

where \bar{m}_i is the modulation index. The maximum modulation index (magnitude), in pu, can be calculated as:

$$m_i^{max} = \sqrt{\frac{3}{2}} \cdot \frac{V_{dc,B}}{2V_{ac,B}} \text{ (pu)} \quad (3)$$

where $V_{dc,B}$ is the DC -voltage base value (pole to pole) and $V_{ac,B}$ is the AC-voltage base value (phase to phase).

2.2 Virtual synchronous machine control (VSM)

A virtual synchronous machine (VSM) is implemented as a supplementary controller that manipulates the set points of the outer controllers of the GF-VSC. Guidelines for the implementation of VSM controllers and different implementations can be found in [5, 7, 21, 23, 35]. This work considers a VSM supplementary controller emulating a classical model of a synchronous machine and equipped with a primary frequency controller, as shown in Fig. 4.

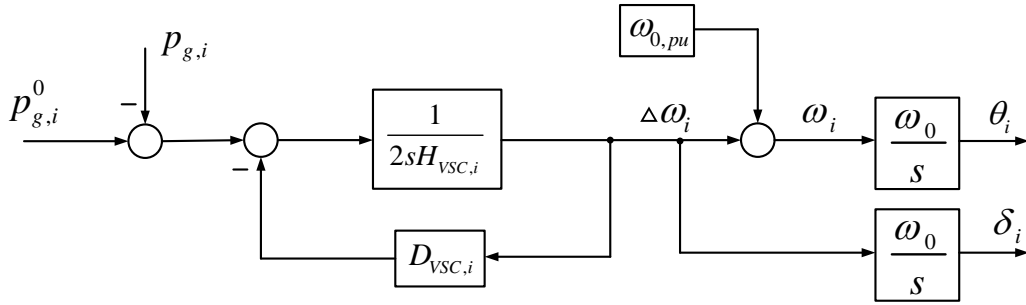


Figure 4: Supplementary controller of a virtual synchronous machine (VSM) implemented in a GF-VSC.

The VSM emulates the swing equation of a synchronous machine:

$$p_{g,i}^0 - p_{g,i} - D_{VSC,i} \Delta\omega_i = 2H_{VSC,i} \frac{d\Delta\omega_i}{dt} \quad (4)$$

where:

- $H_{VSC,i}$ (s) is the emulated inertia constant.
- $D_{VSC,i} = 1/R_{PFR,i}$ (pu) is the proportional gain of the primary frequency controller (or primary frequency response, PFR). It is the inverse of the primary frequency droop constant ($R_{PFR,i}$).
- $\Delta\omega_i = \omega_i - \omega_{0,pu}$ (pu) is the frequency increment of the GF-VSC output frequency, ω_i , with respect to the nominal frequency, $\omega_{0,pu} = 1$ pu.
- $p_{g,i}^0$ (pu) is a constant active-power set point of the GF-VSC at the PCC. This term represents the emulated mechanical power of the VSM.
- $p_{g,i}$ (pu) is the active-power delivered by the GF-VSC measured at the PCC.
- ω_0 is the nominal frequency in rad/s.

Summarising, eventually GF-VSC- i of Fig. 1 will impose the frequency given by the swing equation (Fig. 4 and (4)): ω_i (pu). The emulated rotor angle, δ_i (rad), is the angle of the $d-q$ reference frame (Fig. 3) and θ_i (rad) is the angle used for Park's transformation in Fig. 2. It should be remarked that (4) is a control algorithm imposed by the VSC.

3 Proposed fast voltage boosters to improve transient stability

In this section, fast voltage boosters for GF-VSCs are proposed to improve transient stability. The proposed controllers are based on reactive-power/voltage control in the VSCs and they were inspired by the excitation boosters for synchronous machines proposed in [28–30] to improve transient stability in multi-machine systems.

The active-power injection of the VSC at the connection point (see Fig. 1) can be approximated as:

$$p_{g,i} \simeq \frac{v_{f,i}v_{g,i}}{x_{c,i}} \sin(\delta_{f,i} - \delta_{g,i}) \quad (5)$$

Eq. (5) is useful for qualitative analysis. Loss-of-synchronism in power systems with 100 % of GF-VSC-based generation follows the same pattern as in multi-machine systems with synchronous generators. When a fault occurs, the voltage at the PCC, $v_{g,i}$, is reduced dramatically, reducing the active power injection $p_{g,i}$ (i.e. the virtual electromagnetic torque of the VSC). This produces the acceleration of the VSCs (see the (4)). Depending on the location of the fault, some VSCs will accelerate more than others and severe-enough faults could produce loss of synchronism of GF-VSCs.

Equation (5), shows that the active-power injection can be modified by changing voltage $v_{f,i}$ and this is feasible, since voltage controllers of GF-VSCs have fast responses. Therefore, the voltage set point of each GF-VSC- i can be modified with an additional term ($\Delta v_{f,i}^{ref,TS}$) seeking the improvement of transient stability:

$$v_{f,i}^{ref} = v_{f,i}^0 + \Delta v_{f,i}^{ref,TS} \quad (6)$$

where $v_{f,i}^0$ is the initial voltage set point. Notice that voltage set point $v_{f,i}^{ref}$ is actually the input of the voltage controller (1) (see Fig. 2).

A control strategy will be effective to improve transient stability if it is able to act during the fault and/or immediately after the fault clearing. In fact, VSCs might not be able to produce any effect during the fault, because the converter will limit its current injection, if the fault is close enough.

Transient stability of a single GF-VSC connected to the grid can be improved by slowing down the VSC, following a pattern similar to the one used for a single synchronous machine connected to an infinite grid [26, 27]. Transient stability of a power system with 100 % of GF-VSC-based generation is a more complex phenomenon. A fault will produce that some VSCs accelerate faster than others during the transient and control actions should try to pull their frequency together. In other words, some VSCs will have to be slowed down while others will have to be accelerated. This is, again, analogous to the case of a multi-machine system with conventional synchronous generators, where the use of the speed of the centre of inertia (COI) has proved to be useful [28–30].

The frequency of the COI in a power system with 100 % of GF-VSC-based generation can be defined as [23]:

$$\omega_{COI} = \frac{1}{H_{tot}} \sum_{k=1}^n H_{VSC,k} \omega_k \text{ (pu)}, \text{ with } H_{tot} = \sum_{k=1}^n H_{VSC,k}. \quad (7)$$

Two control strategies are proposed in this work:

- Local fast voltage booster (FVB-L, for short).
- Fast voltage booster using a wide-area control system (WACS) (FVB-WACS, for short).

3.1 Local fast voltage booster (FVB-L)

This control strategy was motivated by previous work on excitation boosters in synchronous machines [27] and on supplementary controllers for transient stability in shunt FACTS devices [31]. It consists in a fast voltage support. Strategy FVB-L uses local measurements as input signals: the voltage at the terminal of VSC- i , $v_{g,i}$, and the frequency deviation of each GF-VSC- i , $\Delta\omega_i = \omega_i - \omega_{0,pu}$ (in pu) and its block diagram is shown in Fig. 5.

The philosophy of local strategy FVB-L is as follows:

- Binary variable $\gamma_{1,i}$ is set to 1 if a voltage sag is detected with an hysteresis, as shown in Fig. 5. If $v_{g,i} \leq v_{A,i}$, then $\gamma_{1,i} = 1$ and remains equal to 1 until $v_{g,i} > v_{B,i}$. If a fault is not detected, then $\gamma_{1,i} = 0$.
- Binary variable $\gamma_{2,i}$ is set to 1 if the frequency deviation of GF-VSC- i (with respect to the nominal frequency) is greater than or equal to a certain threshold: $\Delta\omega_i \geq \omega_{thres,i}$. Otherwise, $\gamma_{2,i} = 0$.
- The supplementary controller is activated with binary variable γ_i , which is the result of a logic circuit with $\gamma_{1,i}$ and $\gamma_{2,i}$ as inputs, as shown in Fig. 5.
- The supplementary voltage set point is given by: $\Delta v_{f,i}^{ref,TS} = \gamma_i \Delta v_{f,i}^{max}$, where $\Delta v_{f,i}^{max} > 0$ is a parameter of the controller ($\gamma_i = 0$ if the controller is deactivated and $\gamma_i = 1$ if the controller is activated).

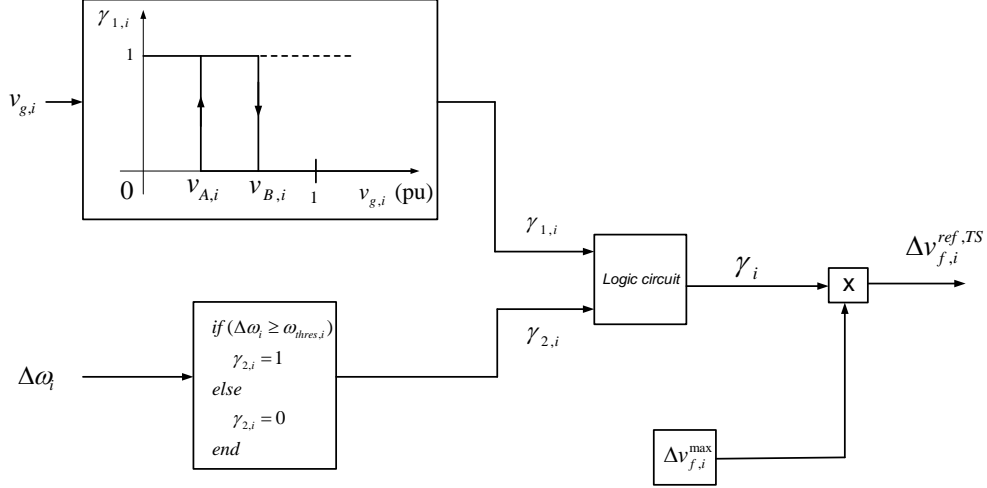


Figure 5: Strategy FVB-L.

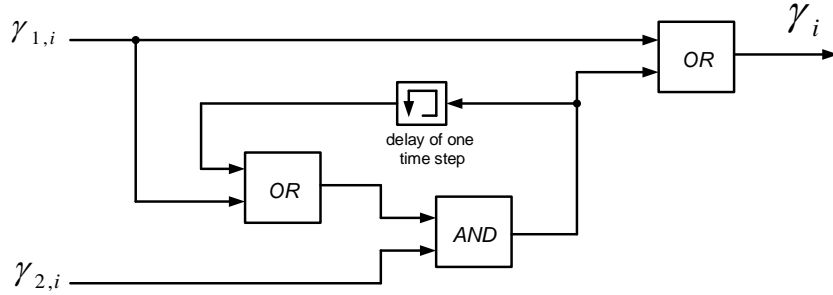


Figure 6: Strategy FVB-L. Logic circuit for fault detection.

The logic circuit rules for the activation of the controller can be summarised as follows:

- The controller will be activated if a voltage sag is detected. Therefore, $\gamma_{1,i}$ will drive the activation of the controller.
- Once the controller is activated, the supplementary voltage set point is maintained if at least one of the two following conditions are satisfied: undervoltage ($\gamma_{1,i} = 1$) or frequency greater than or equal to the threshold ($\gamma_{2,i} = 1$).

With this controller, VSC- i will increase its voltage setpoint with a positive increment $\Delta v_{f,i}^{ref,TS} = \Delta v_{f,i}^{max}$ if it detects a fault, trying to slow down the converter. This mechanism will improve transient stability of the grid-forming VSC connected to the rest of the system. The behaviour of each converter in a power system with several GF-VSCs can be summarised as follows. When a fault occurs, the frequency of all GF-VSCs will increase and all of

them will see a certain voltage sag during the fault. The frequencies of GF-VSCs close to the fault will grow faster than the frequencies of GF-VSCs far from the fault. As discussed previously, the key point in transient stability is the difference between frequencies of the GF-VSCs and not the absolute value of those frequencies. However, with this control strategy, converters do not have this information, because each VSC uses local measurements, only. This problem can be tackled by proper design of thresholds $v_{A,i}$, $v_{B,i}$ and $\omega_{thres,i}$ and with the logic circuit proposed of Fig. 6. With proper design of those thresholds, only controllers of GF-VSCs close to the fault will be activated, and not the ones of VSCs far from the fault. Hence, transient stability in power systems with 100 % of GF-VSC-based generation can be improved.

3.2 Fast voltage booster using a WACS (FVB-WACS)

This control strategy was motivated by previous work on excitation boosters in synchronous machines using the speed of the COI [28–30]. The proposed controller uses a fast voltage booster in each GF-VSC using a wide-area control system (WACS). Following the scheme of Fig. 7, where $K_{FVB,i}$ is a proportional gain, $T_{f,i}$ is a low-pass filter used for noise filtering, $T_{W,i}$ is a wash-out filter used to avoid any control actions in case of steady-state offsets and $\Delta v_{f,i}^{max}$ is a saturation parameter. The input of the controller is the error between a frequency set point ($\omega_i^{ref,TS}$) and the frequency of each GF-VSC (ω_i), in pu. A deadband of $\pm\epsilon_i$ is used to apply the control actions only when the system is subject to large-enough perturbations.

The frequency set point of each VSC- i is calculated as the frequency of the COI (Eq. (7)):

$$\omega_i^{ref,TS} = \omega_{COI} \quad (8)$$

Hence, a communication system is needed.

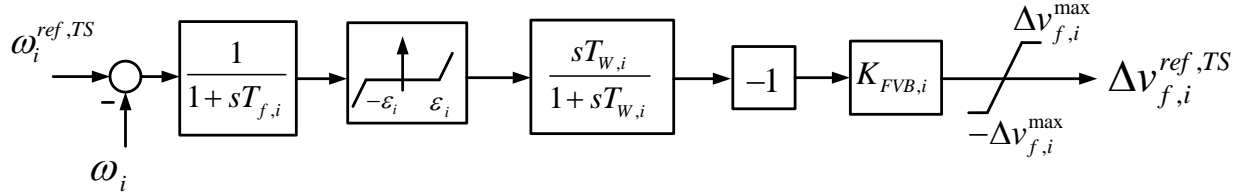


Figure 7: Strategy FVB-WACS.

The philosophy of FVB-WACS controller is as follows:

- If the frequency of VSC- i is above the frequency of the COI, VSC- i will increase its voltage setpoint, trying to slow VSC- i down.
- If the frequency of VSC- i is below the frequency of the COI, VSC- i will decrease its voltage setpoint, trying to accelerate VSC- i .
- Therefore, control actions will pull together the frequencies of GF-VSCs of the system.

4 Results

The behaviour of Kundur's two-area test system [26] with 100% of grid-forming VSC-based generation has been investigated (see Fig. 8). Synchronous machines of the original system were replaced by GF-VSC-based generators with VSM control, with the same rating as the original generators (900 MVA). Data of the system are provided in the Appendix. Simulations were carried out with VSC_Lib tool, an open-source tool based on Matlab + Simulink + SimPowerSystems developed by L2EP-LILLE [37–39]. Average electromagnetic models are used.

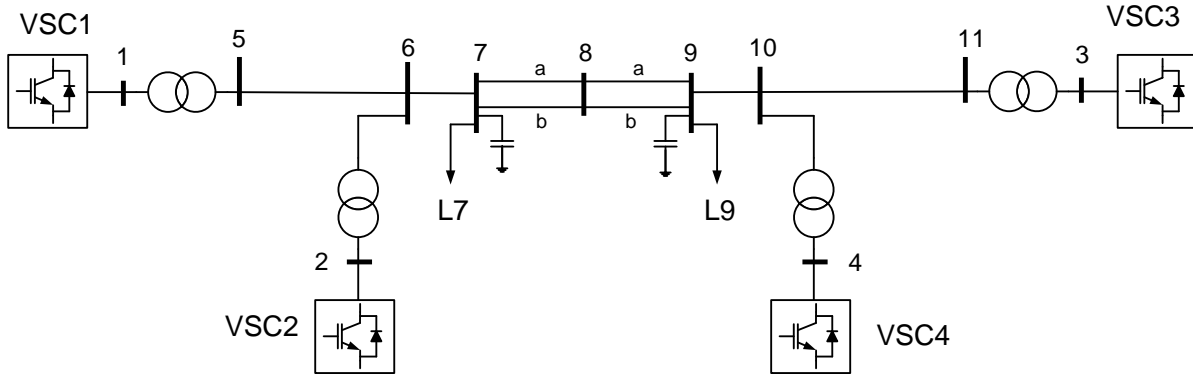


Figure 8: Kundur's two-area test system with 100 % of GF-VSC-based generation.

Table 1 shows the results of the steady-state initial operating point.

Table 1: Initial operating point.

| VSC | $v_{g,i}$ (pu) | $\delta_{g,i}$ (deg) | $P_{g,i}$ (MW) | $Q_{g,i}$ (MVar) |
|-------|----------------|----------------------|----------------|------------------|
| VSC 1 | 1.0475 | 0.44 | 693.00 | 0.00 |
| VSC 2 | 1.0309 | 0.45 | 693.00 | 90.00 |
| VSC 3 | 0.9900 | 0.00 | 642.60 | -69.93 |
| VSC 4 | 0.9738 | 0.16 | 693.00 | 180.00 |

Three cases are compared:

- Base case: no supplementary controller for transient stability is implemented in the GF-VSCs.
- FVB-L: VSCs applying FVB-L strategy (Figs. 5-6), with parameters: $v_{A,i} = 0.75$ pu, $v_{B,i} = 0.9$ pu, $\omega_{thres,i} = 10^{-3}$ pu, $\Delta v_{f,i}^{max} = 0.15$ pu.
- FVB-WACS: VSCs applying FVB-WACS strategy (Fig. 7), with parameters: $K_{FVB,i} = 50$ pu, $T_{f,i} = 0.1$ s, $T_{W,i} = 10$ s, $\Delta v_{f,i}^{max} = 0.15$ pu and $\epsilon_i = 10^{-3}$ pu.

4.1 Short-circuit simulation

A three-phase-to-ground short circuit is applied to line 7-8a (close to bus 7), which is cleared by disconnecting the line 150 ms later (Fault I). Fig. 9 shows the angle difference between VSC-1 and VSC-3. In the base case, VSC-based generators lose synchronism. However, synchronism is maintained with the proposed supplementary controllers FVB-L and FVB-WACS (see Fig. 9).

Fig. 10 shows the frequency deviations of the VSCs with respect to the frequency of the COI, while Fig. 11 shows the supplementary voltage set point provided by the control strategies and the voltages of the VSCs. Notice that local strategy FVB-L is only activated in VSCs 1 and 2, which are close to the fault and not in VSCs 3 and 4, which are far from the fault. This is why strategy FVB-L is also effective in multi-converter systems with 100 % of

grid-forming based generation, and this is the consequence of the logic rules in Fig. 6 and an appropriate design of the controller parameters. In control strategy FVB-WACS, a positive supplementary voltage set point is provided by VSCs 1 and 2 immediately after the fault clearing, because their frequencies are above the frequency of the COI (see Fig. 10). Meanwhile, VSCs 3 and 4 provide a negative supplementary voltage during the first swing, because their frequencies are below the frequency of the COI. Therefore, VSCs 1 and 2 will slow down while VSCs 3 and 4 will accelerate, reducing the risk of loss of synchronism.

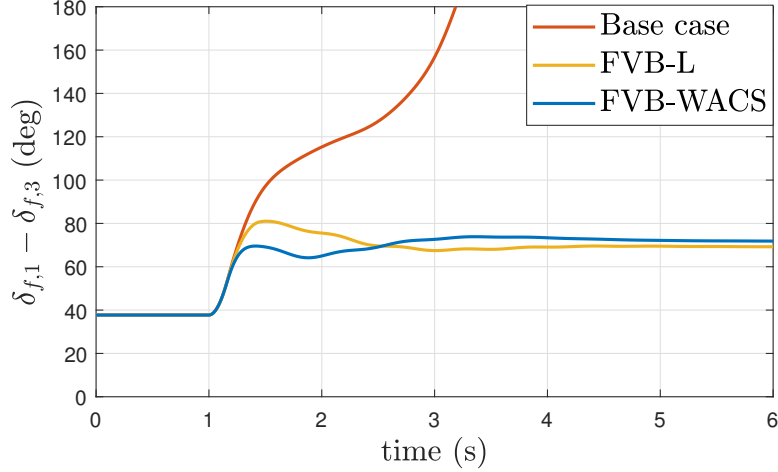


Figure 9: Fault I cleared after 150 ms. Angle difference of the VSCs.

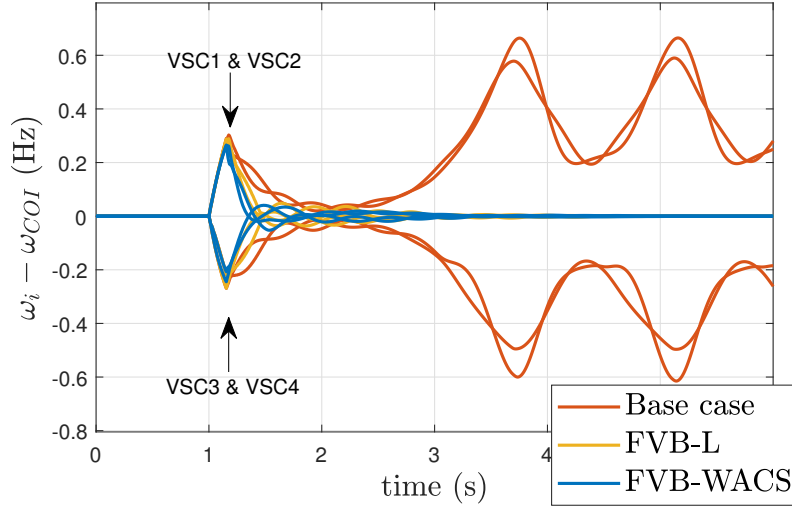


Figure 10: Fault I cleared after 150 ms. Frequency deviations of the VSCs with respect to the frequency of the COI.

Finally, Fig. 12 shows the active-power injections of the VSCs. During the fault, the current limiter leads to variations in the P injections, in order to maintain the current within its limit. After the fault clearing, P injections are affected by the supplementary voltage set point of the proposed control strategies (FVB-L and FVB-WACS). By supplying a positive (negative) additional voltage set point $\Delta v_{f,i}^{ref,TS}$ (Fig. 11), the active-power injection increases (decreases), according to (5). Precisely, (electrical) active-power injections, $p_{g,i}$, drive the slowing down or the acceleration of the GF-VSCs, according to (4).

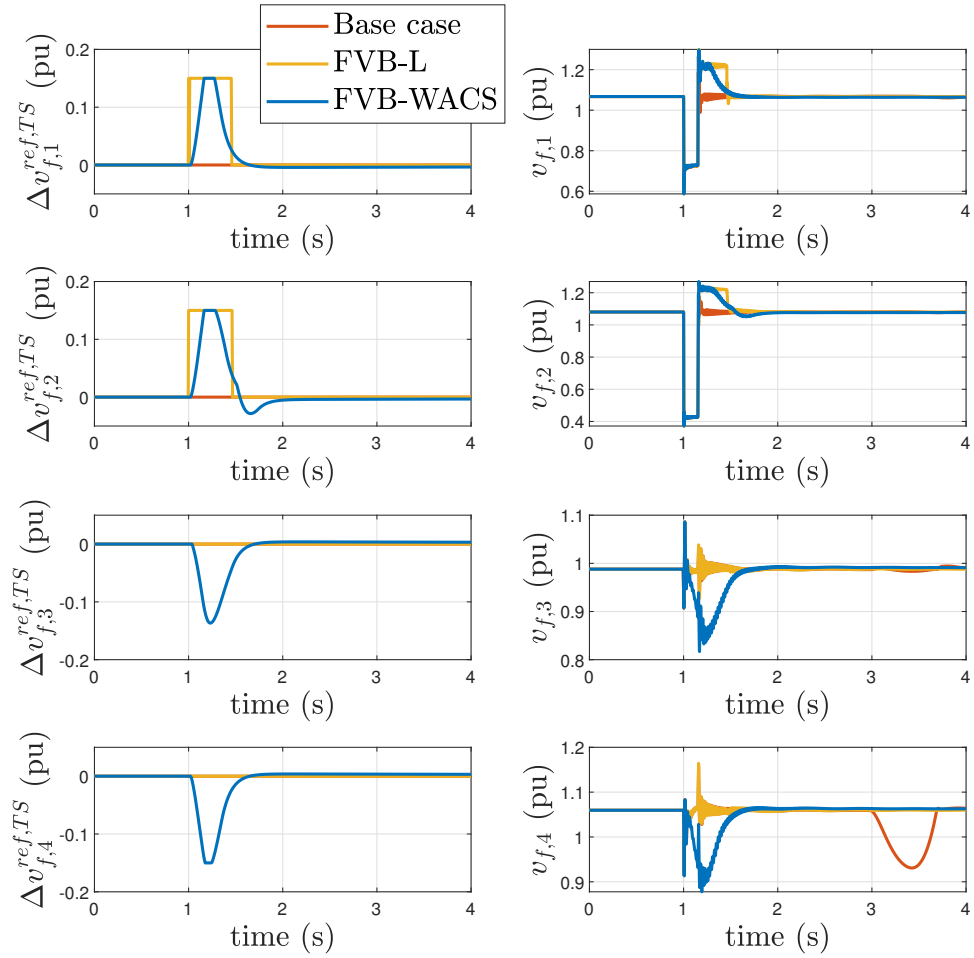


Figure 11: Fault I cleared after 150 ms. (left) Supplementary voltage set points of the VSCs and (right) voltages of the VSCs.

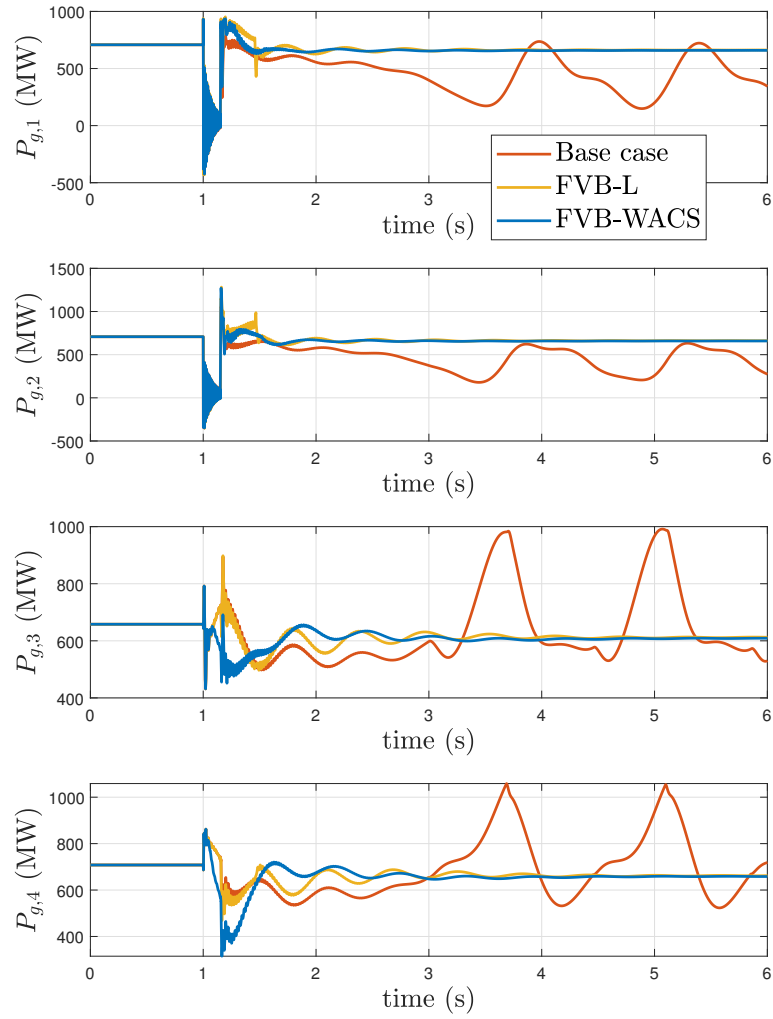


Figure 12: Fault I cleared after 150 ms. Active-power injections of the VSCs.

4.2 Critical clearing times (CCTs) and impact of communication latency

The critical clearing time (CCT) of different faults (described in Table 2) will be used to quantify transient-stability margins. Furthermore, the impact of communication latency on the performance of strategy FVB-WACS will also be analysed. Hence, the input error signal of the supplementary controller of Fig. 7 will be delayed as:

$$u_i = e^{-s\tau}(\omega_{COI} - \omega_i) \quad (9)$$

where τ is the communication delay. The work in [40] reported total communication delays in WACS within the range 50-80 ms. Total communication latency delays of 50 ms and 100 ms will be considered in this work.

CCTs of faults described in Table 2 are given in Table 3. The proposed supplementary controllers FVB-L and FVB-WACS increase the CCT of Fault I significantly. Strategy FVB-L also increases the CCT of Fault II, although the improvement is smaller than the one with strategy FVB-WACS. Furthermore, with strategy FVB-L, the CCT of Fault IV is decreased from 420 ms of the base case to 400 ms. This is due to the conditions of activation of local strategy FVB-L described in Section 3.1. With a proper design of the activation thresholds, this strategy is only activated for severe-enough faults and this is why no negative impact is produced for any fault. For example, if parameter $v_{A,i}$ of Fig. 5 is changed from 0.75 pu to 0.5 pu, the CCT of Fault IV is not reduced (see Table 3). Besides, there could be other faults (e.g. Fault III) in which the control strategies will have no impact. In general, strategy FVB-WACS produces better results than FVB-L. Results of Table 3 also prove that strategy FVB-WACS is robust against communication latency.

Table 2: Fault description

| | Short circuit at line $i - j$ | close to bus | clearing |
|-----------|-------------------------------|--------------|---|
| Fault I | 7-8a | 7 | Disconnect 7-8a |
| Fault II | 5-6 | 5 | short circuit cleared (line not disconnected) |
| Fault III | 10-11 | 11 | short circuit cleared (line not disconnected) |
| Fault IV | 8-9a | 8 | Disconnect 8-9a |

Table 3: Critical clearing times (CCTs).

| CCT (ms) | base case | FVB-L | | FVB-WACS $\tau = 0$ ms | with delay | |
|-----------|-----------|---------------------|--------------------|------------------------|------------|--------|
| | | $v_{A,i} = 0.75$ pu | $v_{A,i} = 0.5$ pu | | 50 ms | 100 ms |
| Fault I | 130 | 250 | 250 | 270 | 270 | 260 |
| Fault II | 270 | 310 | 310 | 360 | 340 | 320 |
| Fault III | 220 | 220 | 220 | 230 | 230 | 230 |
| Fault IV | 420 | 400 | 420 | 880 | 870 | 890 |

4.3 Discussion on the use of local and global measurements

This section discusses two key factors of the proposed control strategies: implementation and effectiveness. In strategy FVB-L, each GF-VSC uses local measurements, only, whereas in strategy FVB-WACS, they use global measurements and, therefore, a communication system is needed. Clearly, the implementation of local strategy FVB-L is easier and cheaper. The ideal control actions are supplying a positive (negative) supplementary voltage in those VSCs with frequency above (below) the frequency of the COI. Although strategy FVB-WACS produces better results than strategy FVB-L, precisely because it uses global measurements (the frequency of the COI), the activation thresholds of the local strategy FVB-L (described Section 3.1) can be tuned in order to ensure that the control strategy is activated only for faults that are close enough, which are, in fact, the ones that produce frequencies above the frequency of the COI. As a general recommendation, local strategy FVB-L can be implemented in grid-forming VSCs to improve transient stability for severe faults. Nevertheless, the use of strategy FVB-WACS could be an interesting option in power systems which are vulnerable to transient stability, since the latter can produce more significant improvements.

5 Conclusions

This paper has proposed two fast voltage boosters to improve transient stability of power systems with 100% of grid-forming VSC-based generation (GF-VSC). One is based on local measurements (FVB-L) and the other one is based on global measurements (FVB-WACS). The conclusions obtained in this paper are as follows:

- Transient-stability phenomenon is present in power systems with 100% of GF-VSC-based generation.
- Local strategy FVB-L improves transient stability of severe faults significantly. However, its control actions must be restricted to severe-enough faults tuning activation thresholds. This means that this control strategy will have little effect on transient stability of non-severe faults.
- Global strategy FVB-WACS improves transient stability, significantly. It produces significant improvements for severe and non-severe faults. The control strategy is robust when subject to communication latency.
- An important advantage of the two control strategies proposed is that they are based on fast voltage control, avoiding changing the set points linked to frequency/active-power injection of the grid-forming VSC (i.e set points linked to the primary energy source of the VSC).

Appendix: data

Data of the grid-forming VSCs are provided in Table 4. Data of the original two-area Kudur's test system can be found in [26]. Nominal voltage of the transmission grid and the nominal frequency (230 kV and 60 Hz, respectively) were changed to 220 kV and 50 Hz in this study. Loads were modelled as constant impedances for dynamic simulation. Besides, a critical case for transient stability was achieved by increasing the power transfer from Area 1 to Area 2:

- Loads: bus 7: 917 MW & 100 MVAR; bus 9: 1817 MW & 100 MVAR.

Table 4: Parameters of the VSCs

| Parameters | |
|--|---|
| VSC's rating are base values for pu | |
| Rating VSC, DC voltage, AC voltage | 900 MVA, ± 320 kV, 300 kV |
| Max. current | 1.25 pu (equal priority for $d - q$ axes) |
| Max. modulation index ($m_i^{max} = \sqrt{\frac{3}{2}} \cdot \frac{V_{dc,B}}{2V_{ac,B}}$) | 1.31 pu |
| Series filter resistance ($r_{f,i}$)/reactance ($x_{f,i}$) | 0.005 pu / 0.15 pu |
| Shunt filter capacitance ($C_{f,i}$) | 0.15 pu |
| Transformer resistance ($r_{c,i}$)/reactance ($x_{c,i}$) (900 MVA 300/220 kV transformer) | 0.005 pu / 0.15 pu |
| Inner prop./int. control ($K_{C,P,i}/K_{C,I,i}$) | 0.73 pu / 1.19 pu/s |
| Outer prop./int. control ($K_{V,P,i}/K_{V,I,i}$) | 0.52 pu / 1.16 pu/s |
| Virtual transient resistance ($r_{V,i}/T_{VR,i}$) | 0.09 pu / 0.0167 s |
| Emulated inertia ($H_{VSC,i}$) of VSCs 1 and 2 | 4.5 s / 4.5 s |
| Emulated inertia ($H_{VSC,i}$) of VSCs 3 and 4 | 4.175 s / 6.175 s |
| Primary freq. controller gain. ($D_{VSC,i}$) | 20 pu |

Acknowledgment

Work supported by the Spanish Government and under RETOS Project Ref. RTI2018-098865-B-C31 (MCI/AEI/FEDER, UE) and by Madrid Regional Government under PROMINT-CM Project Ref. S2018/EMT-4366.

Contact information of the authors

Régulo E. Ávila-Martínez, Javier Renedo, Luis Rouco, Aurelio García-Cerrada and Lukas Sigríst are with the Instituto de Investigación Tecnológica (IIT), ETSI ICAI, Universidad Pontificia Comillas, Madrid, Spain (e-mail: {regulo.avila, javier.renedo, luis.rouco, aurelio, lukas.sigríst}@iit.comillas.edu). Taoufik Qoria and Xavier Guillaud are with the Laboratoire d'Electrotechnique de Puissance (L2EP), Centrale Lille, Arts et Métiers Paris Tech, University of Lille, Lille, France (e-mail: {taoufik.qoria, xavier.guillaud}@centralelille.fr).

References

- [1] J. Rocabert, A. Luna, F. Blaabjerg, and P. Rodríguez, "Control of Power Converters in AC Microgrids," *IEEE Transactions on Power Electronics*, vol. 27, no. 11, pp. 4734–4749, 2012.
- [2] J. M. Guerrero, M. Chandorkar, T.-L. Lee, and P.-C. Loh, "Advanced Control Architectures for Intelligent Microgrids - Part I: Decentralized and Hierarchical Control," *IEEE Transactions on Industrial Electronics*, vol. 60, no. 4, pp. 1254–1262, 2013.
- [3] D. E. Olivares, A. Mehrizi-Sani, A. H. Etemadi, C. A. Canizares, R. Iravani, M. Kazerani, A. H. Hajimiragha, O. Gomis-Bellmunt, M. Seedifard, R. Palma-Behnke, A. Jiménez-Estévez, and N. Hatziaargyriou, "Trends in Microgrid Control," *IEEE Transactions on Smart Grid*, vol. 5, no. 4, pp. 1905–1919, 2014.
- [4] F. Milano, F. Dörfler, G. Hug, D. J. Hill, and Verbič, "Foundations and Challenges of Low-Inertia Systems," in *Proc. Power Systems Computation Conference (PSCC), Dublin, Ireland*, 2018, pp. 1–25.
- [5] M. Paolone, T. Gaunt, X. Guillaud, M. Liserre, S. Meliopoulos, A. Monti, T. Van Cutsem, V. Vittal, and C. Vournas, "Fundamentals of power systems modelling in the presence of converter-interfaced generation," *Electric Power Systems Research*, vol. 189, no. 106811, pp. 1–33, 2020.
- [6] Q.-C. Zhong and G. Weiss, "Synchronverters: Inverters That Mimic Synchronous Generators," *IEEE Transactions on Industrial Electronics*, vol. 58, no. 4, pp. 1259–1267, 2011.
- [7] S. D'Arco, J. A. Suul, and O. B. Fosfo, "A Virtual Synchronous Machine implementation for distributed control of power converters in SmartGrids," *Electric Power Systems Research*, vol. 122, pp. 180–197, 2015.
- [8] J. Roldán-Pérez, A. Rodríguez-Cabero, and M. Prodanovic, "Design and analysis of virtual synchronous machines in inductive and resistive weak grids," *IEEE Transactions on Energy Conversion*, vol. 34, no. 2, pp. 1818–1828, 2019.
- [9] S. D'Arco and J. A. Suul, "Equivalence of Virtual Synchronous Machines and Frequency-Droops for Converter-Based Microgrids," *IEEE Transactions on Smart Grid*, vol. 5, no. 1, pp. 394–395, 2014.
- [10] J. L. Rodríguez Amenedo, S. Arnaltes Gómez, and M. Alonso-Martínez, J González de Armas, "Grid-Forming Converters Control Based on the Reactive Power Synchronization Method for Renewable Power Plants," *IEEE Access*, no. 9, pp. 67 989–68 007, 2021.
- [11] N. Hatziaargyriou, J. V. Milanović, C. Rahmann, V. Ajarapu, C. Canizares, I. Erlich, D. Hill, I. Hiskens, I. Kamwa, B. Pal, P. Pourbeik, J. J. Sanchez-Gasca, A. Stanković, T. Van Cutsem, V. Vittal, and C. Vournas, "Definition and Classification of Power System Stability - Revisited and Extended," *IEEE Transactions on Power Systems*, vol. doi: 10.1109/TPWRS.2020.3041774, pp. 1–12, 2020.
- [12] F. Andrade, J. Cusidó, and L. Romeral, "Transient stability analysis of inverter-interfaced distributed generators in a microgrid system," in *Proc. European Conference on Power Electronics and Applications, Birmingham, UK*, 2011, pp. 1–10.
- [13] F. Andrade, J. Cusidó, L. Romeral, and J. J. Cárdenas, "Study of transient stability for parallel connected inverters in Microgrid system works in stand-alone," in *Proc. World Renewable Energy Congress, BLinköping, Sweden*, 2011, pp. 1–8.

- [14] H. Xin, L. Huang, L. Zhang, Z. Wang, and J. Hu, "Synchronous Instability Mechanism of P-f Droop-Controlled Voltage Source Converter Caused by Current Saturation," *IEEE Transactions on Power Systems*, vol. 31, no. 6, pp. 5206–5207, 2016.
- [15] M. Eskandari and A. V. Savkin, "On the Impact of Fault Ride-Through on Transient Stability of Autonomous Microgrids: Nonlinear Analysis and Solution," *IEEE Transactions on Smart Grid*, vol. doi: 10.1109/TSG.2020.3030015, pp. 1–12, 2020.
- [16] Z. Shuai, C. Shen, X. Liu, Z. Li, and Z. J. Shen, "Transient Angle Stability of Virtual Synchronous Generators Using Lyapunov's Direct Method," *IEEE Transactions on Smart Grid*, vol. 10, no. 4, pp. 4648–4661, 2018.
- [17] H. Cheng, Z. Shuai, C. Shen, X. Liu, Z. Li, and Z. J. Shen, "Transient Angle Stability of Paralleled Synchronous and Virtual Synchronous Generators in Islanded Microgrids," *IEEE Transactions on Power Electronics*, vol. 35, no. 8, pp. 1019–1033, 2020.
- [18] D. Pan, X. Wang, F. Liu, and R. Shi, "Transient Stability of Voltage-Source Converters With Grid-Forming Control: A Design-Oriented Study," *IEEE Journal of Emerging and Selected Topics in Power Electronics*, vol. 8, no. 2, pp. 1019–1033, 2020.
- [19] T. Qoria, F. Gruson, F. Colas, X. Kestelyn, and X. Guillaud, "Current limiting algorithms and transient stability analysis of grid-forming VSCs," *Electric Power Systems Research*, vol. 189, no. 106726, pp. 1–8, 2020.
- [20] T. Qoria, F. Gruson, F. Colas, G. Denis, T. Prevost, and X. Guillaud, "Critical Clearing Time Determination and Enhancement of Grid-Forming Converters Embedding Virtual Impedance as Current Limitation Algorithm," *IEEE Journal of Emerging and Selected Topics in Power Electronics*, vol. 8, no. 2, pp. 1050–1061, 2020.
- [21] T. Qoria, E. Rokrok, A. Bruyere, B. Francois, and X. Guillaud, "A PLL-Free Grid-Forming Control With Decoupled Functionalities for High-Power Transmission System Applications," *IEEE Access*, no. 106765, pp. 197 363–197 378, 2020.
- [22] C. Shen, Z. Shuai, Y. Shen, Y. Peng, X. Liu, Z. Li, and J. Shen, "Transient Stability and Current Injection Design of Paralleled Current-Controlled VSCs and Virtual Synchronous Generators," *IEEE Transactions on Smart Grid*, vol. doi: 10.1109/TSG.2020.3032610, pp. 1–15, 2020.
- [23] M. Choopani, S. H. Hosseinian, and B. Vahidi, "New Transient Stability and LVRT Improvement of Multi-VSG Grids Using the Frequency of the Center of Inertia," *IEEE Transactions on Power Systems*, vol. 35, no. 1, pp. 527–538, 2020.
- [24] X. Xiong, C. Wu, P. Cheng, and F. Blaabjerg, "An Optimal Damping Design of Virtual Synchronous Generators for Transient Stability Enhancement," *IEEE Transactions on Power Electronics*, vol. doi: 10.1109/TPEL.2021.3074027, pp. 1–5, 2021.
- [25] D. C. Lee and P. Kundur, "Advanced excitation controls for power system stability enhancement," in *CIGRE*, no. 38-01, 1986.
- [26] P. Kundur, *Power System Stability and Control*. McGraw Hill Education, 1994.
- [27] L. Díez-Maroto, L. Rouco, and F. Fernández-Bernal, "Modeling, sizing and control of an excitation booster for enhancement of synchronous generators fault ride through capability: experimental validation," *IEEE Transactions on Energy Conversion*, vol. 31, no. 4, pp. 1304–1314, 2019.
- [28] L. Díez-Maroto, L. Vanfretti, M. S. Almas, G. M. Jónsdóttir, and L. Rouco, "A WACS exploiting generator Excitation Boosters for power system transient stability enhancement," *Electric Power Systems Research*, vol. 148, pp. 245–253, 2017.
- [29] L. Díez-Maroto, J. Renedo, L. Rouco, and F. Fernández-Bernal, "Lyapunov Stability Based Wide Area Control Systems for Excitation Boosters in Synchronous Generators," *IEEE Transactions on Power Systems*, vol. 34, no. 1, pp. 194–204, 2019.
- [30] —, "Wide area controllers for excitation boosters for transient stability improvement," *Electric Power Systems Research*, vol. 189, no. 106622, pp. 1–6, 2020.

- [31] M. H. Haque, "Improvement of First Swing Stability Limit by Utilizing Full Benefit of Shunt FACTS Devices," *IEEE Transactions on Power Systems*, vol. 19, no. 4, pp. 1894–1902, 2004.
- [32] A. Fuchs, M. Imhof, T. Demiray, and M. Morari, "Stabilization of Large Power Systems Using VSC-HVDC and Model Predictive Control," *IEEE Transactions on Power Delivery*, vol. 29, no. 1, pp. 480–488, 2014.
- [33] J. Renedo, A. García-Cerrada, and L. Rouco, "Reactive-Power Coordination in VSC-HVDC Multi-Terminal Systems for Transient Stability Improvement," *IEEE Transactions on Power Systems*, vol. 32, no. 5, pp. 3758–3767, 2017.
- [34] T. Qoria, F. Gruson, F. Colas, X. Guillaud, M.-S. Debry, and T. Prevost, "Tuning of cascaded controllers for robust grid-forming Voltage Source Converter," in *Proc. Power Systems Computation Conference (PSCC), Dublin, Ireland*, 2018, pp. 1–8.
- [35] E. Rokrok, T. Qoria, A. Bruyere, B. Francois, and X. Guillaud, "Classification and dynamic assessment of droop-based grid-forming control schemes: Application in HVDC systems," *Electric Power Systems Research*, vol. 189, no. 106765, pp. 1–7, 2020.
- [36] G. S. Pereira, V. Costan, A. Bruyère, and X. Guillaud, "Simplified approach for frequency dynamics assessment of 100% power electronics-based systems," *Electric Power Systems Research*, vol. 188, no. 106551, pp. 1–8, 2020.
- [37] L2EP-LILLE, "VSC_Lib: Grid Forming Models for Matlab/SimPowerSystem," vol. <https://github.com/l2ep-epmlab/> (accessed 08-07-2020), 2020.
- [38] T. Qoria, Q. Cossart, C. Li, X. Guillaud, F. Colas, F. Gruson, and X. Kestelyn, "WP3-Control and Operation of a Grid with 100% Converter-Based Devices. Deliverable 3.2: Local control and simulation tools for large transmission systems," MIGRATE Project, Tech. Rep., 2018.
- [39] T. Qoria, F. Gruson, F. Colas, G. Denis, T. Prevost, and X. Guillaud, "Inertia effect and load sharing capability of grid forming converters connected to a transmission grid," in *Proc. 15th IET International Conference on AC and DC Power Transmission (ACDC), Coventry, UK*, 2019, pp. 1–6.
- [40] F. Zhang, Y. Sun, L. Cheng, X. Li, J. H. Chow, and W. Zhao, "Measurement and Modeling of Delays in Wide-Area Closed-Loop Control Systems," *IEEE Transactions on Power Systems*, vol. 30, no. 1, pp. 2426–2433, 2015.